PAPER

Check for updates

Phenyl selenoxide functionalized TPA/TPE π-conjugated imidazo[1,2-*a*]pyridine: a fluorescent probe for the selective detection of water in organic solvents

Jerome Issac,[a] R. Rameshbabu Priyadharsan,[b] Kamalanathan Chidambaranathan,[a] Subramanian Karthikeyan,[c] Dohyun Moon, [ID] *[d] Savarimuthu Philip Anthony [ID] *[b] and Vedichi Madhu [ID] *[a]

Phenyl selenoxide functionalized tetraphenylethylene (TPE) and triphenylamine (TPA) electron donors π-conjugated with the imidazo[1,2-*a*]pyridine acceptor, namely, *N*,*N*-diphenyl-4-(3-(phenylseleninyl) imidazo[1,2-*a*]pyridin-2-yl)aniline (**SeO-TPA**) and 3-(phenylseleninyl)-2-(4-(1,2,2-triphenylvinyl)phenyl) imidazo[1,2-*a*]pyridine (**SeO-TPE**), were synthesized, and the effect of TPA/TPE on their photophysical properties was explored. **SeO-TPA** showed emission in both solution and solid states, while **SeO-TPE** exhibited emission only in the solid state. **SeO-TPA** also exhibited solvent polarity-dependent emission due to a hydrophilic Se=O group. Interestingly, the selenoxide of **SeO-TPA** reacted with a trace amount of water present in the organic solvents and produced dihydroxy selenane derivatives. The structural transformation of selenoxide (**SeO-TPA**) to dihydroxy selenane (**Se(OH)$_2$-TPA**) resulted in fluorescence changes from 448 nm to 420 nm. The reduction of electron-withdrawing character by converting selenoxide to dihydroxy selenane resulted in a blue shift of the emission. The concentration-dependent studies of **SeO-TPA** indicated that the probe can detect water in organic solvents up to 0.429 wt% in CH$_3$CN, 0.602 wt% in ethanol, 1.108 wt% in DMF, 0.514 wt% in DMSO, and 1.028 wt% in THF. Hence, this work reported on a naked-eye detectable fluorescence probe for sensing trace amounts of water in organic solvents, highlighting its potential applications in environmental and analytical chemistry.

Introduction

Water is a transparent, colorless, and odorless liquid with several unique physicochemical properties, such as a high dielectric constant, large heat capacity, and high surface tension. These properties render water essential for a wide range of applications in various scientific and industrial domains. Notably, water is a common contaminant in organic solvents, impacting chemical processes in various industries such as laboratory chemistry, fine chemicals, food production, pharmaceuticals and influences photovoltaic performance.[1-4] This contamination can greatly impact chemical reactivity, product quality, yield, and overall reliability. Even small

amounts of water in the reaction medium can pose substantial safety risks, particularly in industries such as pharmaceutical manufacturing, chemical synthesis, and food production.[5-8] Consequently, developing methods for the qualitative and quantitative detection of water in organic solvents has gained great importance in various industrial processes. The Karl Fischer titration is the primary method utilized for the quantitative analysis of water content in organic solvents.[9-12] This method demonstrates reduced sensitivity to aprotic and non-alcoholic solvents. In addition, several instrumental methods, including gas chromatography (GC), nuclear magnetic resonance (NMR), UV-visible absorption spectroscopy, Fourier transform infrared spectroscopy (FT-IR), and electrochemical techniques, are employed to detect and quantify water content in organic solvents.[13-17] In this context, the development of optical probes (both colorimetric and fluorometric) offers several advantages. These include simplicity, high sensitivity and selectivity, fast response times, ease of operation, good biocompatibility, and visible color changes that can be detected by the naked eye. Notably, this approach is also non-destructive. Specifically, fluorescent sensors designed for detecting trace amounts of water in organic solvents are highly attractive due to

[a]Multifunctional Materials and Catalysis Laboratory, Division of Physical Sciences, Karunya Institute of Technology and Sciences, Coimbatore-641 114, Tamil Nadu, India. E-mail: madhu@karunya.edu; vmadhuu1@gmail.com; Tel: +914222614483

[b]School of Chemical & Biotechnology, SASTRA University, Thanjavur-613401, Tamil Nadu, India. E-mail: philip@biotech.sastra.edu; Tel: +914362264101

[c]PG and Research Department of Chemistry, Khadir Mohideen College (affiliated to Bharathidasan University), Adirampattinam, Tamil Nadu, India

[d]Beamline Department, Pohang Accelerator Laboratory, 80 Jigokro-127 beongil, Nam-gu, Pohang, Gyeongbuk, Korea. E-mail: dmoon@postech.ac.kr

their selectivity, high sensitivity, and rapid response.[18–25] Several fluorescence probes have already been developed for water sensing. These fluorescence probes are designed based on various mechanisms, including intramolecular charge transfer (ICT),[26,27] excited-state intramolecular proton transfer (ESIPT),[28] photo-induced electron transfer (PET),[29–31] aggregation-induced emission (AIE),[32] solvatochromism,[33,34] and water-induced proton transfer.[35,36] In general, water can act as both a proton donor and acceptor, influencing processes such as proton or charge transfer, aggregation, protonation, and hydrogen bonding. These processes can significantly alter the optoelectronic properties of molecules. Specifically, for donor–π–acceptor (D–π–A) structures, the ICT band is notably affected by solvent polarity.[37] The presence of water can alter the polarity, hydrogen bonding, or viscosity of the solution, which could affect the optical properties of ICT-type sensors, making it a valuable strategy for detecting water in organic solvents.[38–40]

The previous literature reports suggest that selenoxides can be chemically transformed into dihydroxy selenanes in an aqueous environment (Scheme 1).[41,42] The change in electronic environments resulting from the conversion of selenides to selenoxides and dihydroxy selenanes may significantly influence the optical band gap and fluorescence properties. The water-sensitive chemical transformation and modulation of electronic energy levels could be leveraged to develop fluorescence probes for detecting trace amounts of water in organic solvents. Although the chemical transformation is known, no fluorescence probes based on water-reactive selenoxides for water sensing have been reported to date.

In this manuscript, we designed and synthesized selenium integrated triphenylamine (TPA)/tetraphenylethylene (TPE) imidazo derivatives (**Se-TPA** and **Se-TPE**) and converted them to the corresponding selenoxide-functionalized fluorophores for the detection or/and sensing of water in various organic solvents. The selenide fluorophore dyads, **Se-TPA** and **Se-TPE**, were converted to their selenoxides, **SeO-TPA** and **SeO-TPE**, using hydrogen peroxide (H_2O_2) as the oxidizing agent (Scheme 1 and 2).

The selenoxides exhibited distinct fluorescence properties. These selenoxides were subsequently transformed into dihydroxy selenanes in the presence of water in organic solvents, which resulted in significantly different fluorescence characteristics. The formation of dihydroxy selenanes, along with their fluorescence response, was utilized for sensing trace amounts of water in organic solvents. Specifically, **SeO-TPA** showed the capability of sensing water in the range from 9.56 to 27.85 μL or 4780 μL L^{-1} to 13 925 μL L^{-1} in various organic solvents.
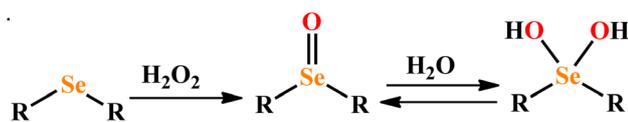
Scheme 1 The catalytic cycle demonstrates the oxidation of selenides to selenoxides, followed by their reaction with water to produce dihydroxy selenanes.
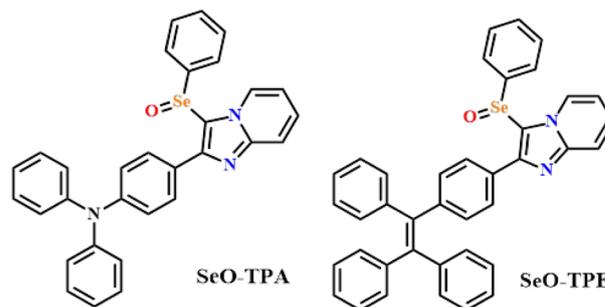
Scheme 2 The molecular structures of **SeO-TPA** and **SeO-TPE** used in this study.

Experimental

Materials and methods

All solvents and chemicals were sourced from reputable commercial suppliers, including Aldrich, TCI, Merck, Avra, and HiMedia, and were used as received. When necessary, solvents were purified using appropriate drying agents. Fourier-transform infrared (FT-IR) measurements were conducted using a Shimadzu IR Affinity-1S spectrophotometer with KBr pellets. NMR spectra were recorded on a Bruker Avance 400 MHz FT-NMR spectrometer. UV-vis absorption spectra were obtained with a UV-vis-NIR spectrophotometer (Jasco V-770). Liquid chromatography-mass spectrometry (LC-MS) was performed on an Agilent 1260 Infinity II system, combined with an InfinityLab LC/MSD iQ mass detector (ESI). Single crystals were coated with paratone-N oil, and diffraction data were measured using synchrotron radiation on an ADSC Quantum-210 detector at the 2D SMC facility, employing a silicon (111) double crystal monochromator (DCM) at the Pohang Accelerator Laboratory in Korea. Crystallographic data for **Se-TPE** have been deposited at the Cambridge Crystallographic Data Centre under supplementary publication numbers CCDC-2491312. These data can be accessed free of charge from the Cambridge Crystallographic Data Centre at **https://www.ccdc.cam.ac.uk/data_request/cif**.

Synthesis of Se-TPA

Diphenyldiselenide (0.085 g, 0.5 mmol) and a catalytic quantity of iodine (5 mol%) were added to a solution of 4-(imidazo[1,2-a]pyridin-2-yl)-N,N-diphenylaniline (0.2 g, 1 mmol) in DMSO (2 mL). The reaction mixture was heated at 90 °C with stirring for 9 hours in a pressure tube under a nitrogen atmosphere. The completion of the reaction was monitored by TLC. After the reaction was complete, the reaction mixture was cooled to room temperature and extracted using CH_2Cl_2 and water. The organic layer was separated and dried over anhydrous sodium sulfate. Following the evaporation of the solvent, the crude mixture was purified by column chromatography using ethyl acetate : hexane (5 : 95) as the eluent, resulting in the formation of a brown powder as the final product. Yield (0.160 g, 55%). FT-IR (KBr): ν (cm^{-1}) = 3547, 2925, 2850, 1575, 1477, 1310, 1269, 827, 732. ^{1}H NMR (400 MHz, CDCl$_3$): δ 8.35–8.33 (d, 1H, J = 6 Hz), 8.06–8.03 (d, 3H, J = 9 Hz), 7.73–7.70 (d, 2H, J = 9 Hz), 7.33–7.31 (d, 2H, J

= 6 Hz), 7.15–7.13 (t, 11H, J = 6 Hz), 7.05–7.03 (d, 2H, J = 6 Hz), 6.87–6.85 (t, 23H, J = 6 Hz). ^{13}C NMR (100 MHz, CDCl$_3$): δ 151.47, 148.13, 147.66, 147.58, 131.04, 129.71, 129.53, 129.29, 128.07, 127.32, 126.63, 126.51, 125.54, 124.77, 123.14, 122.81, 117.31, 112.96, 102.14. LC-MS (CH$_3$CN) m/z calcd for C$_{31}$H$_{23}$N$_3$Se: 517.105, found: 516.350 [M − H]$^+$.

Synthesis of SeO-TPA

A suspension of *N,N*-diphenyl-4-(3-(phenylselanyl)imidazo[1,2-*a*]pyridin-2-yl)aniline (0.155 g, 3 mmol) in acetonitrile (10 mL) was treated with a slow addition of aqueous hydrogen peroxide (4 mL, 35%). The resulting mixture was then heated to 90 °C with stirring for 3 h, and TLC analysis indicated significant conversion. The mixture was allowed to cool to room temperature and was then partitioned between dichloromethane and saturated aqueous sodium bicarbonate. The organic phase was separated, and the aqueous phase was extracted thrice with dichloromethane. The combined organic extract was dried and concentrated under vacuum, yielding a crude product that was purified by column chromatography using ethyl acetate : hexane (7 : 93) to afford the desired product as a pale yellow powder. Yield (0.090 g, 58%). FT-IR (KBr): ν (cm^{-1}) = 3461, 2920, 2853, 1645, 1436, 1162, 697. ^{1}H NMR (400 MHz, CDCl$_3$): δ 8.36–8.33 (d, 1H, J = 9 Hz), 7.76–7.73 (d, 3H, J = 9 Hz), 7.54–7.51 (d, 2H, J = 9 Hz), 7.30–7.27 (t, 3H, J = 9 Hz), 7.22–7.19 (t, 5H, J = 9 Hz), 7.10–7.07 (t, 3H, J = 9 Hz), 7.00–6.97 (d, 6H, J = 9 Hz). ^{13}C NMR (100 MHz, CDCl$_3$): δ 165.34, 151.91, 151.55, 147.22, 146.69, 138.73, 135.20, 129.60, 128.71, 125.91, 125.76, 124.41, 120.59, 114.52. LC-MS (CH$_3$CN) m/z calcd for C$_{31}$H$_{23}$N$_3$OSe: 533.10, found: 534.1500 [M + H]$^+$.

Synthesis of Se-TPE

Diphenyldiselenide (0.07 g, 0.5 mmol) and a catalytic quantity of iodine (5 mol%) were added to a solution of 2-(4-(1,2,2-triphenylvinyl)phenyl)imidazo[1,2-*a*]pyridine (0.2 g, 1 mmol) in DMSO (2 mL). The reaction mixture was heated at 90 °C with stirring for 9 hours in a pressure tube under a nitrogen atmosphere. The completion of the reaction was monitored by TLC. After the reaction was complete, the reaction mixture was cooled to room temperature and extracted using CH$_2$Cl$_2$ and water. The organic layer was separated and dried over anhydrous sodium sulfate. Following the evaporation of the solvent, the crude mixture was purified by column chromatography using ethyl acetate : hexane (4 : 96) as the eluent, affording a brown coloured powder as the final product. Yield (0.170 g, 63%). FT-IR (KBr): ν (cm^{-1}) = 3430, 3056, 2920, 1631, 1442, 1335, 1022, 749, 695. ^{1}H NMR (400 MHz, CDCl$_3$): δ = 8.33–8.31 (d, 1H, J = 6 Hz), 7.94–7.91 (d, 2H, J = 9 Hz), 7.69–7.66 (d, 1H, J = 9 Hz), 7.32–7.29 (d, 2H, J = 9 Hz), 7.16–7.14 (t, 3H, J = 6 Hz), 7.11–7.10 (t, 5H, J = 3 Hz), 7.09–7.07 (d, 8H, J = 6 Hz) 7.04–7.02 (t, 5H, J = 6 Hz), 6.86–6.83 (t, 1H, J = 9 Hz). ^{13}C NMR (100 MHz, CDCl$_3$): δ = 151.47, 147.69, 143.95, 143.82, 143.69, 143.60, 141.29, 140.66, 131.75, 131.48, 131.38, 130.90, 129.66, 128.32, 128.00, 127.79, 127.67, 127.64, 126.68, 126.54, 126.43, 125.56, 117.41, 112.96, 102.81. LC-MS (CH$_3$CN) m/z calcd for C$_{39}$H$_{28}$N$_2$Se: 604.14, found: 605.130 [M + H]$^+$.

Synthesis of SeO-TPE

A suspension of 3-(phenylseleninyl)-2-(4-(1,2,2-triphenylvinyl)phenyl)imidazo[1,2-*a*]pyridine (0.155 g, 0.25 mmol) in 10 mL of acetonitrile was treated with a slow addition of aqueous hydrogen peroxide (4 mL, 35%), and the resulting mixture was heated to 90 °C with stirring for 3 h. TLC analysis indicated significant conversion. The mixture was allowed to cool to room temperature, and was then partitioned between dichloromethane and saturated aqueous sodium bicarbonate. The organic phase was separated, and the aqueous phase was extracted thrice with dichloromethane. The combined organic extract was dried and concentrated under vacuum, yielding a crude product that was purified by column chromatography using ethyl acetate : hexane (9 : 91) to afford the desired product as a bright yellow powder. Yield (0.095 g, 62%). FT-IR (KBr): ν (cm^{-1}) = 3447, 2925, 2853, 1678, 1427, 1306, 749, 6 85. ^{1}H NMR (400 MHz, CDCl$_3$): δ = 9.71–9.70 (d, 1H, J = 3 Hz), 8.46–8.43 (d, 1H, J = 9 Hz), 8.27–8.25 (d, 2H, J = 6 Hz), 7.83–7.80 (t, 3H, J = 9 Hz), 7.11–7.10 (d, 11H, J = 3 Hz), 7.06–7.05 (t, 10H, J = 3 Hz). ^{13}C NMR (100 MHz, CDCl$_3$): δ = 151.85, 149.00, 148.17, 146.75, 143.27, 143.14, 142.46, 140.02, 139.85, 139.16, 131.63, 131.29, 129.48, 127.86, 127.72, 127.12, 126.93, 126.74, 119.75, 115. LC-MS (CH$_3$CN) m/z calcd for C$_{39}$H$_{28}$N$_2$OSe: 620.14, found: 620.350 [M + H]$^+$.

Result and discussion

Triphenylamine (TPA) and tetraphenylethylene (TPE) π-conjugated imidazo[1,2-*a*]pyridine based donor–acceptor compounds, TPA-IP and TPE-IP, were synthesized following the previously reported procedure from our research group.[43] The reaction of diphenyldiselenide with TPA-IP/TPE-IP in the presence of iodine as a catalyst in DMSO at 90 °C for 9 h resulted in the formation of the desired 3-phenylselanylimidazo[1,2-*a*]pyridine compounds, **Se-TPA** and **Se-TPE** (Scheme 3).

Se-TPA and **Se-TPE** were characterized using FT-IR spectroscopy, ^{1}H and ^{13}C nuclear magnetic resonance (NMR) and mass spectrophotometry analyses. In order to investigate the influence of substituents on the structure–property relationship, efforts were made to grow single crystals of **Se-TPA** and **Se-TPE** using a different crystallization method. However, single crystals of **Se-TPE** alone were successfully obtained from
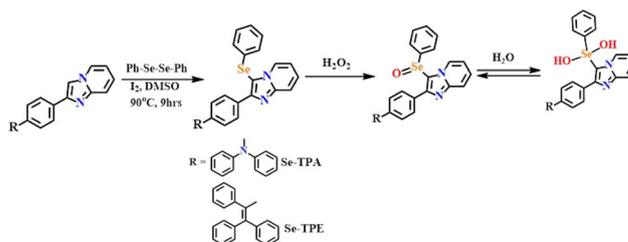
Scheme 3 The catalytic cycle demonstrates the oxidation of selenides, **Se-TPA** and **Se-TPE**, to selenoxides, **SeO-TPA** and **SeO-TPE**, which then react with water to yield the dihydroxy selenanes, Se(OH)$_2$-TPA and Se(OH)$_2$-TPE.

a dichloromethane–hexane solvent mixture. Single-crystal structural analysis of **Se-TPE** demonstrated that it crystallizes in the monoclinic space group $P2_1/c$. The single-crystal structure of **Se-TPE** is presented in Fig. 1a, with relevant crystallographic information provided in Table S1. The crystal structure analysis revealed that the TPE unit of **Se-TPE** exhibited a twisted molecular conformation, which could hinder close molecular $\pi\cdots\pi$ stacking in the crystal lattice. Furthermore, **Se-TPE** formed a supramolecular rectangular structure, facilitated by intermolecular C–H$\cdots$N hydrogen bonding interactions between the imidazo[1,2-a]pyridine and tetraphenylethylene moieties, as shown in Fig. 1b. The C–H$\cdots$N hydrogen bonding interactions (C31–H31$\cdots$N1) exhibited H$\cdots$N distances of 2.739 Å and the bond angle is 138.78°. The twisted molecular units of TPA and TPE are expected to show aggregation induced/ enhanced emission in the solid-state.

Consequently, the solid-state fluorescence properties of **Se-TPA** and **Se-TPE** were investigated at room temperature. **Se-TPA** exhibited fluorescence at 422 nm, while **Se-TPE** showed fluorescence at 436 nm (Fig. 2). **Se-TPE** displayed stronger fluorescence than **Se-TPA**, which may be due to the structural rigidification caused by the twisted structure of the TPE unit and intermolecular interactions.

Moreover, the fluorescence of both **Se-TPA** and **Se-TPE** was investigated in the solution state. **Se-TPA** exhibited strong fluorescence in both polar protic and aprotic solvents. The compound, **Se-TPA** displayed blue fluorescence at ∼426 nm in solution. In contrast, **Se-TPE** showed no fluorescence in solution. TPE is a well-known example of an aggregation-induced emission (AIE) luminophore.[44] Additionally, its propeller-like structure restricts intramolecular rotation (RIR), which promotes non-radiative energy decay and results in weak or absent fluorescence in the solution state.[45] Organo-selenide compounds are susceptible to oxidation by hydrogen peroxide
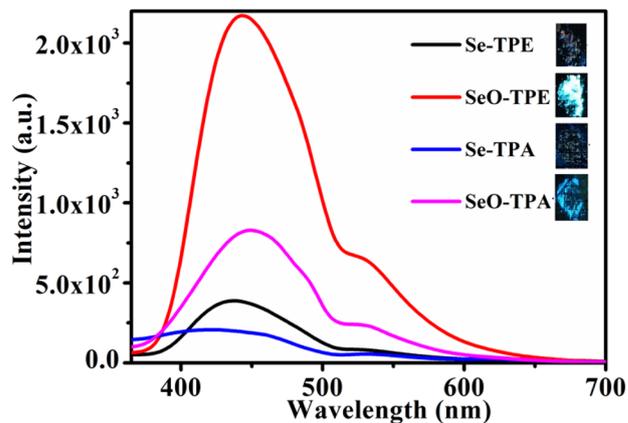

Fig. 2 Solid-state emission spectra of **Se-TPE** (black), **Se-TPA** (blue), **SeO-TPA** (purple), and **SeO-TPE** (red). (Inserts) Fluorescence images in the solid states under UV (365 nm) irradiation.

(H_2O_2), which results in the formation of the corresponding selenoxides.[41,42] Therefore, in this study, we assessed the oxidation of both **Se-TPA** and **Se-TPE** using hydrogen peroxide (H_2O_2) in acetonitrile (CH_3CN) at room temperature. The oxidation of **Se-TPA** to **SeO-TPA** was monitored through changes in fluorescence. In CH_3CN, **Se-TPA** displayed blue fluorescence before oxidation, which changed to green fluorescence within five minutes of reaction with hydrogen peroxide (Fig. 3).

The reaction of **Se-TPA** with H_2O_2 was also monitored using thin-layer chromatography (TLC), which indicated the formation of a new compound. This new product was then separated and characterized through ^{1}H and ^{13}C NMR spectroscopy, as well as mass spectrometry. The NMR spectra of the newly formed product displayed changes in the chemical shift values from the original **Se-TPA**. Additionally, the mass spectrum showed an $[M + H]^+$ peak at m/z 534.150, confirming the formation of **SeO-TPA**. The combined NMR and mass spectrometric analyses confirms the formation of **SeO-TPA** from **Se-TPA** during the oxidation process with H_2O_2.

The emission studies were conducted for **SeO-TPA** in various solvents to further evaluate the impact of structural change on its emission properties in solution (Fig. 4 and S17). Unlike **Se-TPA**, **SeO-TPA** exhibited tunable emission depending on the solvent polarity (Fig. 4b). It is noted that **Se-TPA** exhibited a consistent emission color across the solvent polarity (Fig. 4a).
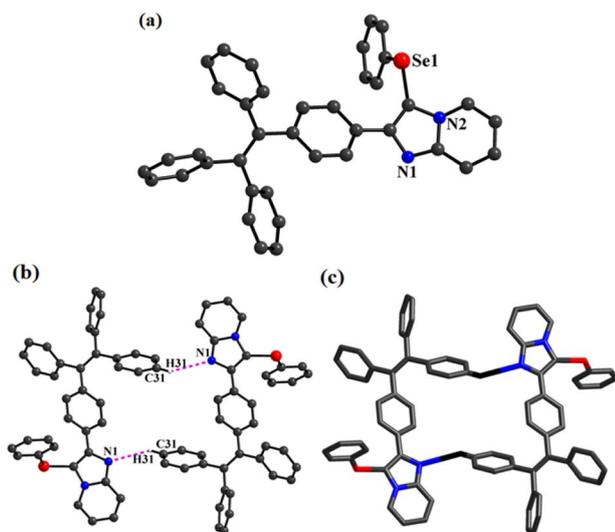

Fig. 1 (a) Structure of a single crystal of **Se-TPE**, supramolecular rectangular structure mediated by intermolecular C–H$\cdots$N hydrogen bonding interactions. (b) Ball and stick. (c) Wireframe representations.
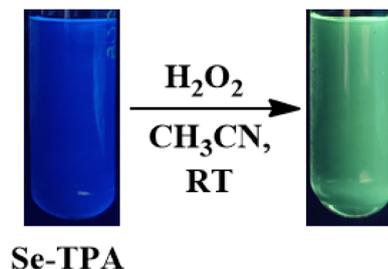

Fig. 3 Visual fluorescence color changes of **Se-TPA** (1×10^{-5} M) upon oxidation to H_2O_2 under UV (365 nm) irradiation.
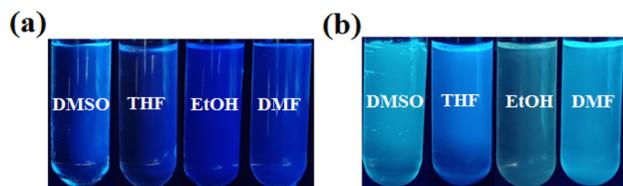
Fig. 4 Photographic images demonstrating the solvent-dependent emission behavior of (a) **Se-TPA** and (b) **SeO-TPA** in various solvents (1.0×10^{-5} M).

The solvent polarity-dependent behavior suggests that **SeO-TPA** is more polar in nature than **Se-TPA**. Similarly, the selenoxide **SeO-TPE** was synthesized from **Se-TPE** through oxidation with H_2O_2. The solid-state fluorescence spectra for **Se-TPA**, **Se-TPE**, **SeO-TPA**, and **SeO-TPE** are presented in Fig. 2. The spectra show that both **SeO-TPA** and **SeO-TPE** displayed red-shifted emission bands, with enhanced intensity at 450 nm for **SeO-TPA** and 444 nm for **SeO-TPE**. In comparison, **Se-TPA** and **Se-TPE** exhibited emission bands at 422 nm and 436 nm, respectively. The observed red shifts in the emission of **SeO-TPA** and **SeO-TPE** can be attributed to the increased electron-withdrawing effect of the Se=O group.

Computational studies were performed to gain insight into tuning the optical band gap by converting selenides to selenoxides. The highest occupied molecular orbital (HOMO) of both **Se-TPE** and **Se-TPA** showed that the electron density was primarily concentrated in the donor TPE/TPA unit (Fig. 5). In the lowest unoccupied molecular orbital (LUMO), the electro density spread the whole structure in **Se-TPE**. However, it showed significant transfer of electron density to the 3-(phenylselanyl)imidazo[1,2-*a*]pyridine unit in **Se-TPA**. The

comparison of the HOMO–LUMO energy gaps revealed a relatively low band gap for **Se-TPA** (3.61 eV) than that for **Se-TPE** (3.73 eV). After oxidation, **SeO-TPE** and **SeO-TPA** exhibited optical band gaps of 3.71 eV and 3.59 eV, respectively, which are quite similar to the optical band gaps of **Se-TPE** and **Se-TPA**. The optical band gaps for both compounds were slightly reduced after converting the selenides to selenoxides. HOMO–LUMO revealed a similar electron density transfer from the donor TPE/TPA into the acceptor imidazo-pyridine unit.

The reduction of optical band gaps supported the red shifting of fluorescence while converting from selenide to selenoxide derivatives. The selenoxide compounds are known to convert to dihydroxy selenanes when reacting/contacting with water.[41,42] This transformation can alter the electronic energy levels and consequently affect the fluorescence properties of the fluorophore. Thus, **SeO-TPA** was chosen to investigate the water-sensitive fluorescence modulation since it also showed strong fluorescence in solution state (Scheme 3). As expected, the π-conjugated selenoxide fluorophore **SeO-TPA** exhibited fluorescence modulation upon reacting with water, leading to the formation of **Se(OH)₂-TPA**.

The fluorescence modulation from reacting with water was exploited as a probe for the visual detection of trace water in

Fig. 6 (a) The effect of water addition on **SeO-TPA** (10^{-5} M) emission in CH_3CN. (b) The limit of water detection in CH_3CN.
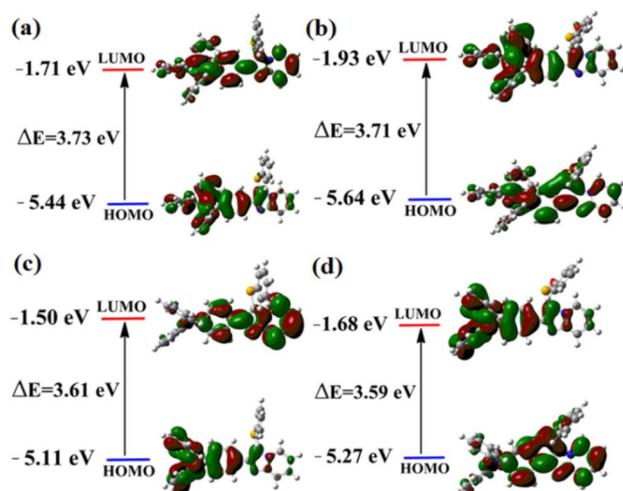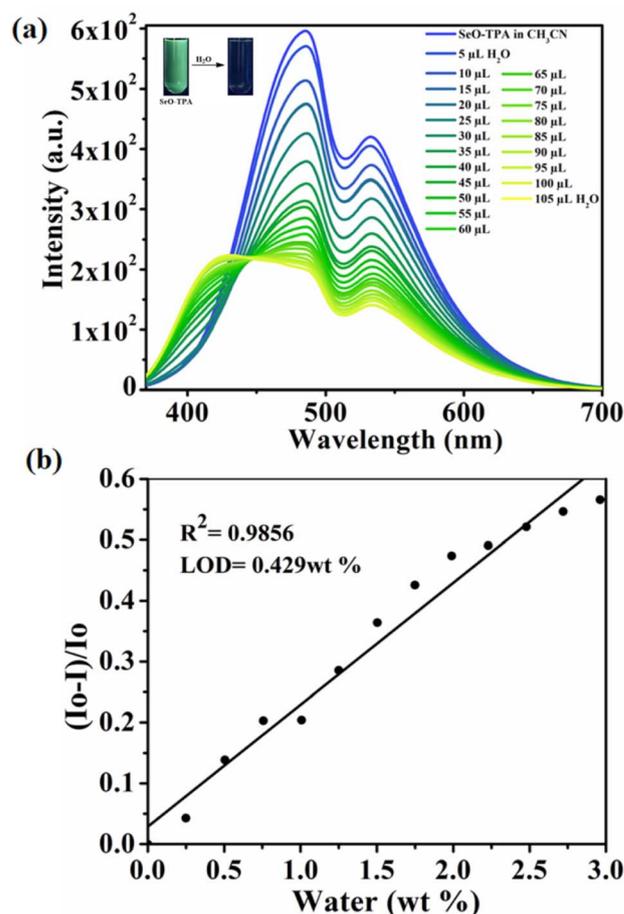

Fig. 5 The optimized ground-state distributions of the HOMO and LUMO, along with their corresponding energy values and the optical band gap, were obtained through density functional theory (DFT) calculations using the B3PW91/6-31+G(d,p) model for the following compounds: (a) **Se-TPA**, (b) **SeO-TPE**, (c) **Se-TPA**, and (d) **SeO-TPA**.

various organic solvents. **SeO-TPA** showed green emission in CH_3CN (Fig. 6a). The fluorescence color was changed from green to light blue upon the addition of water. The change of emission indicated the conversion of **SeO-TPA** into **Se(OH)$_2$-TPA**. The conversion of Se=O to Se(OH)$_2$ is expected to shift from a smaller energy gap to a larger energy gap (**SeO-TPA**) (ΔE) > SeOH$_2$-TPA (ΔE). In this reaction, Se=O reacts with water to produce Se(OH)$_2$, which can then lose a water molecule to revert back to Se=O. Hence, both Se=O and Se(OH)$_2$ exist in equilibrium.[41] It is noted that the TPA–Se=O peak fluorescence intensity was reduced with the emergence of a new blue-shifted peak by the addition of water. This further supported the presence of Se=O and Se(OH)$_2$ in equilibrium. The concentration-dependent studies revealed that 5 µL water addition itself showed a significant decrease of fluorescence intensity at 488 and 533 nm. As the concentration of water increased, both emission bands gradually decreased. The emission bands at 488 and 533 nm were almost quenched after adding 105 µL of water. The limit of detection (LOD) studies indicated that **SeO-TPA** can effectively sense water concentrations as low as 0.429 wt% in CH_3CN (Fig. 6b). To broaden the scope of the water sensing property of the **SeO-TPA** probe, fluorescence modulation in different organic solvents were

explored. In DMF and DMSO, the **SeO-TPA** solution changed color from sky blue to navy blue upon the addition of water. In pure DMF, **SeO-TPA** exhibited strong fluorescence peaks at 456 nm and 526 nm (Fig. 7a). The intensity of both peaks was reduced upon adding water. Digital fluorescence images also confirmed the decrease of fluorescence intensity with increasing water percentages. The limit of detection (LOD) analysis revealed that water can be detected up to 1.108 wt% in DMF (Fig. 7b).

A similar fluorescence variation was also observed in DMSO. The LOD analysis indicated that the **SeO-TPA** probe is capable of detecting water content up to 0.514 wt% in DMSO (Fig. S18). **SeO-TPA** in THF exhibited a strong emission at 438 nm, accompanied by a shoulder peak at a longer wavelength of 530 nm (Fig. S19). The intensity of the emission peaks gradually decreased with increasing water addition. This demonstrates that the water-sensitive chemical transformation of fluorescent selenoxide can be successfully used for the selective sensing of trace amounts of water in organic solvents. In biological systems, understanding the reduction of Se=O to Se(OH)$_2$ is essential for comprehending selenium's role in various biochemical processes. Conjugating a fluorophore to the Se=O moiety offers a viable method for monitoring selenium metabolism *in vivo*, thus providing insights into glutathione peroxidases (GPx) mimetics. Moreover, this type of probe shows significant promise for observing oxygen-transfer catalysis involving Se=O. Additionally, it is particularly advantageous for both qualitative and quantitative assessments of water content in diverse organic solvents, which has important implications for various industrial applications.

Conclusion

In summary, we have synthesized TPE/TPA integrated selenide derivatives, **Se-TPE** and **Se-TPE**, and converted them into the corresponding selenoxides, **SeO-TPE** and **SeO-TPA**. All four compounds showed donor-dependent tunable solid-state fluorescence. Furthermore, **Se-TPA** and **SeO-TPA** exhibited strong fluorescence in solution. The selective water reaction of selenoxide coupled with the solution fluorescence property of **SeO-TPA** was utilized for highly selective trace amount water sensing in organic solvents. **SeO-TPA** selenoxide was converted to dihydroxy selenane **Se(OH)$_2$-TPA** and disruption of π-conjugation led to fluorescence changes. The modulation of the fluorescence of **SeO-TPA** was used for highly selective trace water sensing in organic solvents. Water-dependent fluorescence studies indicated that **SeO-TPA** can effectively sense water up to 0.429 wt% in CH_3CN, 0.602 wt% in ethanol, 1.108 wt% in DMF, 0.514 wt% in DMSO, and 1.028 wt% in THF. Thus, the present work demonstrated the development of a water-sensing fluorescence probe by making use of its reactivity.
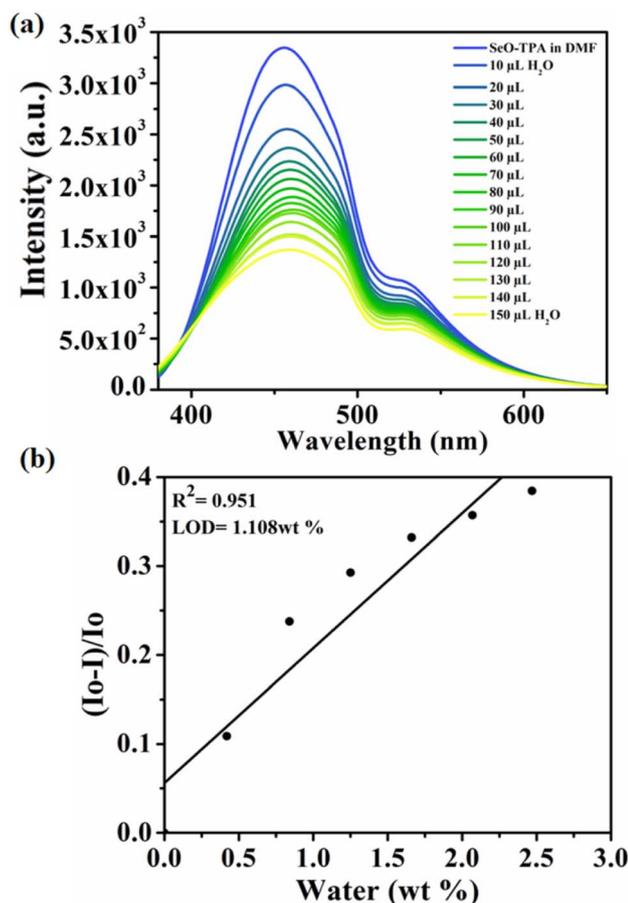

Fig. 7 (a) The effect of water addition on **SeO-TPA** (10^{-5} M) emission in DMF. (b) The limit of water detection in DMF.

Conflicts of interest

There are no conflicts to declare.

Data availability

CCDC 2491312 contains the supplementary crystallographic data for this paper.[46]

The data supporting this article have been included as part of the SI. Supplementary information: synthesis, ^{1}H and ^{13}C NMR spectra, FT-IR spectra, mass spectra, photophysical studies and crystal data and structural refinement details for the compound **Se-TPE**. See DOI: https://doi.org/10.1039/d5ra07283b.

Acknowledgements

References

1 M. Trigo-Lopez, A. Munoz, S. Ibeas, F. C. García, F. Serna and J. M. García, *Sens. Actuators, B*, 2014, **191**, 233–238.

2 F. Yang, E. Feng, Y. Han, C. Zhang, J. Chang, H. Li, J. Shi, Q. Luo, C.-Q. Ma and J. Yang, *J. Phys. Chem. Lett.*, 2025, **16**, 9052–9061.

3 Q. Deng, Y. Li, J. Wu, Y. Liu, G. Fang, S. Wang and Y. Zhang, *Chem. Commun.*, 2012, **48**, 3009–3011.

4 Z. Zhao, Q. Hu, W. Liu, X. Xiong, Z. Wang and H. Wang, *Dyes Pigm.*, 2023, **213**, e111186.

5 R. Das, S. Bej, H. Hirani and P. Banerjee, *ACS Omega*, 2021, **6**, 14104–14121.

6 T. I. Kim and Y. Kim, *Anal. Chem.*, 2017, **89**, 3768–3772.

7 L. A. Frink and D. W Armstrong, *J. Pharmacol. Sci.*, 2016, **105**, 2288–2292.

8 Y. Roggo, V. Pauli, M. Jelsch, L. Pellegatti, F. Elbaz, S. Ensslin, P. Kleinebudde and M. Krumme, *J. Pharm. Biomed. Anal.*, 2020, **179**, e112971.

9 Y. Y. Liang, *Anal. Chem.*, 1990, **62**, 2504–2506.

10 P. Lam and M. Nariman, *Pharm. Technol.*, 2009, **33**, 52–60.

11 N. Dantan, W. Frenzel and S. Küppers, *Talanta*, 2000, **52**, 101–109.

12 L. Liu, Q. Zhang, H. Duan, C. Li and Y. Lu, *Anal. Methods*, 2021, **13**, 3792–3798.

13 K. Wan, M. Li, T. Huang, W. Zhang, T. Zhang, X. Li, H. Wang and J. Lv, *Anal. Chem.*, 2023, **95**, 15673–15680.

14 R. Velvarská, M. Fiedlerová, J. M. Hidalgo-Herrador and Z. Tisler, *Spectrosc. Lett.*, 2019, **52**, 1–8.

15 E. Kang, H. R. Park, J. Hoon, H. Y. Yu, S. K. Chang, B. Kim, K. Choi and S. Ahn, *Microchem. J.*, 2018, **138**, 395–400.

16 S. B. H. Lang, E. Azizi, J. Aromandi, D. Nematollahi and A. R. Massah, *New J. Chem.*, 2018, **42**, 14926–14932.

17 Z. Fan, K. Zhang, X. Feng, Y. Hu, Z. Chen, S. Wang, J. Liu and B. Zhang, *J. Electroanal. Chem.*, 2024, **970**, 118556.

18 J. Wang, Y. Huang, Z. Gao and J. Du, *ACS Appl. Nano Mater.*, 2024, **7**, 7958–7965.

19 Y. Mise, K. Imato, T. Ogi, N. Tsunoji and Y. Ooyama, *New J. Chem.*, 2021, **45**, 4164–4173.

20 H. Dai, Z. Xu, K. Yang, J. Zhou, J. Wang, Y. Zhang, Y. Shen, X. Liu, Y. Jiang and W. Xu, *Inorg. Chem.*, 2024, **63**, 24351–24362.

21 J. Wu, C. Li, Q. Chen, L. Xu, M. Jiana and J. Zhao, *J. Mater. Chem. C*, 2022, **10**, 10595–10608.

22 P. Kumar, R. Kaushik, A. Ghosh and D. A. Jose, *Anal. Chem.*, 2016, **88**, 11314–11318.

23 Y. Zhang, D. Li, Y. Li and J. Yu, *Chem. Sci.*, 2014, **5**, 2710–2716.

24 T. Chen, Z.-Q. Chen, W.-L. Gong, C. Li and M.-Q. Zhu, *Mater. Chem. Front.*, 2017, **1**, 1841–1846.

25 Z. Huang, F. Tang, A. Ding, F. He, R.-H. Duan, J. Huang, L. Konga and J. Yang, *Mol. Syst. Des. Eng.*, 2022, **7**, 963–968.

26 A. Morimoto, K. Shimizu, N. Suzuki, S. Yagi, K. Sueyoshi, T. Endo and H. Hisamoto, *Analyst*, 2024, **149**, 1939–1946.

27 S. Tsumura, T. Enokia and Y. Ooyama, *Chem. Commun.*, 2018, **54**, 10144–10147.

28 H. L. Qian, C. Dai, C. X. Yang and X. P. Yan, *ACS Appl. Mater. Interfaces*, 2017, **9**, 24999–25005.

29 Y. Ooyama, K. Furue, K. Uenakaa and J. Ohshita, *RSC Adv.*, 2014, **4**, 25330–25333.

30 E. Nishimoto, Y. Mise, T. Fumoto, S. Miho, N. Tsunoji, K. Imato and Y. Ooyama, *New J. Chem.*, 2022, **46**, 12474–12481.

31 S. Miho, T. Fumoto, Y. Mise, K. Imato, S. Akiyama, M. Ishidab and Y. Ooyama, *Mater. Adv.*, 2021, **2**, 7662–7670.

32 F. Duarte, G. Dobrikov, A. Kurutos, H. M. Santos, J. Fernández-Lodeiro, J. Luis, C. -Martinez, E. Oliveira and C. Lodeiro, *Dyes Pigm.*, 2023, **218**, 111428.

33 L. Ding, Z. Zhang, X. Lib and J. Su, *Chem. Commun.*, 2013, **49**, 7319–7321.

34 Y. Zhang, C. Lianga and S. Jiang, *New J. Chem.*, 2017, **41**, 8644–8649.

35 W. Pan, C. Zheng, G. Liao, G. Liu and S. Pu, *Microchem. J.*, 2021, **163**, 105887.

36 L. McDonald, J. Wang, N. Alexander, H. Li, T. Liu and Y. Pang, *J. Phys. Chem. B*, 2016, **120**, 766–772.

37 X. Ma, X. Jin, H. Bai, L. Ma, X. Li, X. Fang, W. Chen and M. She, *Spectrochim. Acta, Part A*, 2024, **308**, 123791.

38 A. Morimoto, K. Shimizu, N. Suzuki, S. Yagi, K. Sueyoshi, T. Endo and H. Hisamoto, *Analyst*, 2024, **149**, 1939–1946.

39 L. McDonald, J. Wang, N. Alexander, H. Li, T. Liu and Y. Pang, *J. Phys. Chem. B*, 2016, **120**, 766–772.

40 Y. Ooyama, H. Egawa and K. Yoshida, *Eur. J. Org Chem.*, 2008, 5239–5243.

41 V. Nascimento, E. E. Alberto, D. W. Tondo, D. Dambrowski, M. R. Detty, F. Nome and A. L. Braga, *J. Am. Chem. Soc.*, 2012, **134**, 138–141.

42 G. Ribaudo, M. Bellanda, I. Menegazzo, L. P. Wolters, M. Bortoli, G. Ferrer-Sueta, G. Zagotto and L. Orian, *Chem. Eur. J*, 2017, **23**, 2405–2422.

43 J. Issac, S. Ravi, K. Chidambaranathan, S. Karthikeyan, M. Pannipara, A. G. Al-Sehemi, S. P. Anthony and V. Madhu, *Cryst. Growth Des.*, 2024, **24**, 3388–3398.

44 J. Luo, Z. Xie, J. W. Y. Lam, L. Cheng, H. Chen, C. Qiu, H. S. Kwok, X. Zhan, Y. Liu, D. Zhuc and B. Z. Tang, *Chem. Commun.*, 2001, 1740–1741.

45 J. Mei, N. L. C. Leung, R. T. K. Kwok, J. W. Y. Lam and B. Z. Tang, *Chem. Rev.*, 2015, **115**, 11718–11940.

46 CCDC 2491312: Experimental Crystal Structure Determination, 2025, DOI: **10.5517/ccdc.csd.cc2pmdxn**.